Chapter 3

Elastic scattering for $^{6}Li+^{51}V$ and systematic study of breakup threshold anomaly

3.1 Introduction

3.2 Experimental setup

3.3 Experimental and Theoretical Analysis

3.3.1 Optical Model Analysis

3.3.2 Microscopic Double Folding model analysis

3.3.3 Dispersion Calculation

3.3.4 CDCC Analysis

3.4 Systematic studies

3.4.1 Systematics of Dispersion Calculation

3.4.2 Systematics of Reaction Cross-Section

3.5 Summary and Conclusion

3.1 Introduction

Weakly bound projectiles (WBP) make a remarkable difference in their interaction with target nuclei by possessing alpha cluster structure, producing α-particles through the breakup, transfer, and pick up from targets, the transfer is followed by the breakup, sequential breakup, complete fusion of all fragments, etc. The study of reactions induced by WBP shares common characteristics like cluster structure and low breakup threshold with exotic nuclei. Thus an organized comprehension of reaction process (breakup, transfer) opens the door to studying exotic nuclei derived from primordial nucleosynthesis [1].Reactions near the Coulomb barrier like elastic/inelastic scattering, transfer, and breakup incorporating exotic and weakly bound nuclei, give analytical sight for involved degrees of freedom. When compared to weakly bound stable nuclei, exotic beams are still accessible at low currents. Therefore, weakly bound stable nuclei constitute an important preliminary step towards understanding exotic ones. The elastic scattering of WBP with variant target mass represents a variation in potential behavior owing to the variable significance of Coulomb and nuclear breakups as well as the inclusion of other reaction channel coupling effects. Generally, Light projectiles are preferred to maintain low Coulomb dominance rather than heavy nuclei projectiles [2]. In the present work, we have taken ^{6}Li as WBP with a target of ^{51}V in a light mass region. The breakup threshold for $^{6}\text{Li} \rightarrow \alpha + n + p$ is 3.7 MeV but its 3^{+} and 0^{+} resonance are 2.19 MeV and 3.56 MeV respectively. These can lead to resonant breakup as well. The associated relevance of these channels will be determined by the target + projectile states' energy balance and angular momentum [3, 4]. The first excited

state of ^{51}V is 1.609 MeV which is quite above the breakup threshold of 1.475 MeV of ^{6}Li, thus target inelastic state is not significant here and only coupling to break up and transfer channels are of primary importance for the $^{6}Li+^{51}V$ system [5].

3.2 Experimental Measurements

The experimental work was performed using a General Purpose Scattering Chamber (GPSC) of 14UD Pelletron-LINAC accelerator facility at TIFR, Mumbai. Section 2.1 gives an schematic layout of accelerator and reference [6] gives a detailed description of the accelerator functioning. This facility can generate accelerated beams of nuclear particles such as protons, α- particles, and various types of heavy ions with sufficient energies to investigate numerous nuclear processes in the low energy regime.The measurement was done using a $^{6}Li^{3+}$ ion beam bombarded with energies 14, 20, 23, 26 MeV between current range 5-28 nA on self-supported 1.17 mg/cm^2 thick ^{51}V target. A rectification of beam energies for half thickness of target were performed during scrutiny. This accounts for a deduction of ∼280 keV to ∼400 keV for 26 MeV to 14 MeV energy range. Identification of charged particles was done with the help of silicon surface barrier detectors on ΔE+E telescope arrangement covering 14° to 170° angular range. Figure 3.1 shows the experimental arrangement of detectors and detailed physics for semiconductor detectors can be revisited in section 2.2. For beam monitoring and absolute normalization, 300 μm thick two surface barrier monitor detectors were mounted at ±10°. Detectors thickness were, T1 (ΔE=40μm, E=1mm), T2 (ΔE=27μm, E=1 mm), T3 (ΔE=25μm, E=2mm), and T4 (ΔE=25μm,E=1mm). 'Linux-based data acquisition system LAMPS' was utilized for data

recording [7]. Figure 3.2 demonstrate a typical particle spectrum for $^{6}Li+^{51}V$ system at E_{lab} = 25.7 MeV and lab angle 40°. We have included angular distribution at lower energies from reference [8] to describe the energy behavior of potential nearby the Coulomb barrier whereas author showed interest to study the significance of spectroscopic deformations of isotopes of Li.

3.3 Experimental and Theoretical analysis

Elastic scattering angular distribution studies were undertaken applying a microscopic double folding model and phenomenological optical model. The radius of sensitivity is calculated using optical model analysis and energy dependence of potential can be calculated from dispersion relation. Apart from the above, the effect of breakup coupling is explored with CDCC calculations in upcoming sections.

3.3.1 Optical Model analysis

SFRESCO module of FRESCO code, version FRES 3.1 [9] gave a satisfactory description of elastic scattering data. Well known Woods – Saxon form of potential was deployed to extract dependence of potential parameters on energy. This way obtained best fitted parameters are represented in figure 3.3 fitted values are given in Table 3.1, where real (v) and imaginary (w) radii are defined by $R_{v,\,w}= r_{v,w}(A^{1/3}_{P}+A^{1/3}_{T})$ fm,, V_0,W_0 are real and imaginary potential depths, $a_{v,\,w}$ diffuseness parameter, respectively, σ_R is reaction cross-section are listed. The acceptable

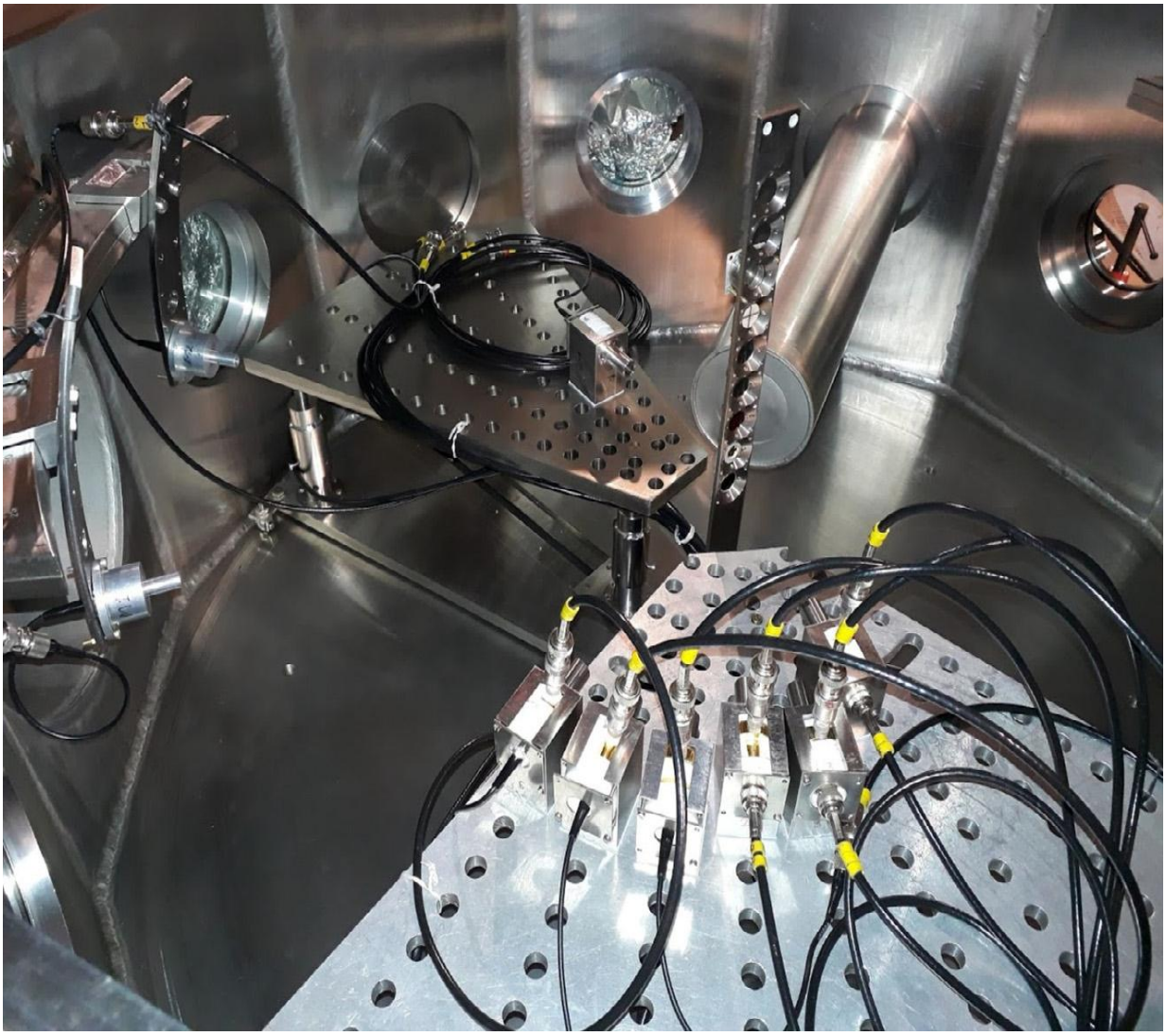

Figure 3.1: *Photograph of mounting arrangement for detector telescopes (T1, T2, T3, and T4), Monitors (M1, M2), target ladder, and Faraday cup (outside the chamber).*

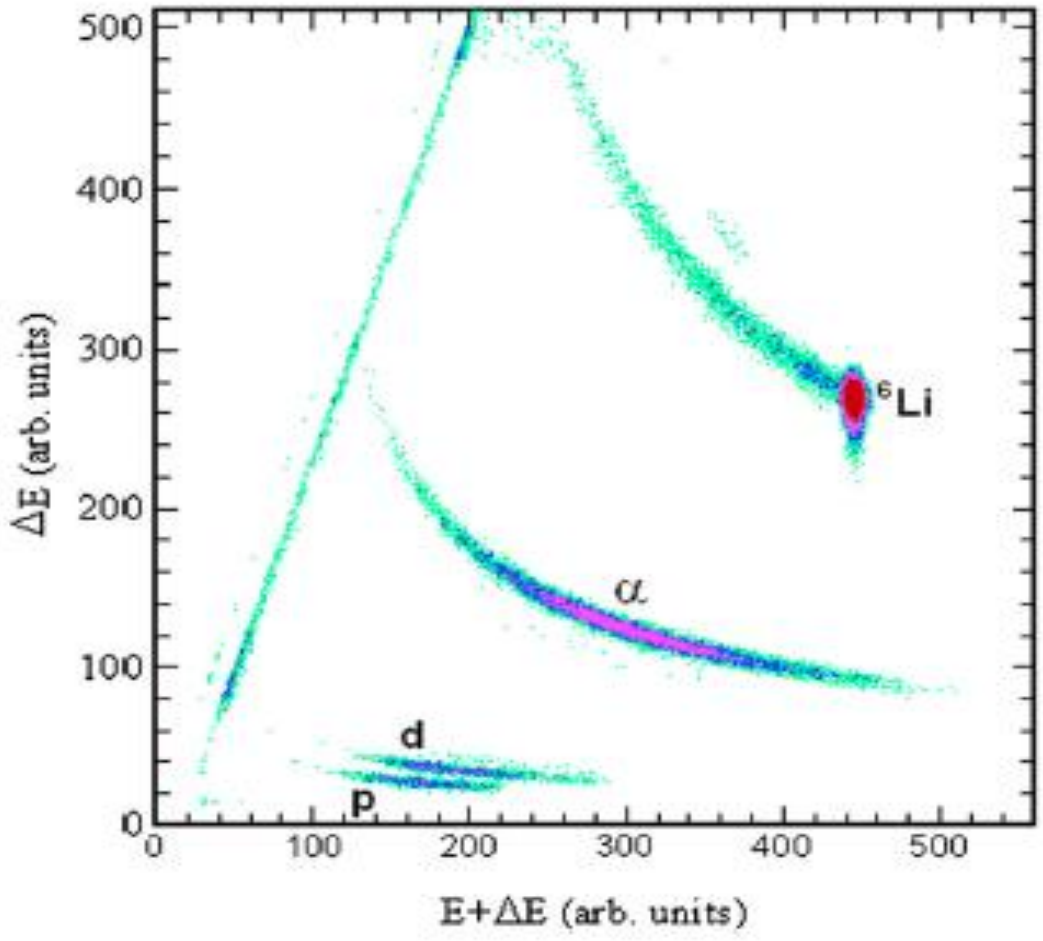

Figure 3.2: *Particle ΔE-(E+ΔE) spectrum at E_{lab}=25.7MeV, θ_{lab}=40°, for the system $^{6}Li+^{51}V$.*

values of fitting are within χ^2 range where $\chi^2 = \chi^2_{min} \pm \chi^2_{min}/2$. The errors obtained in reaction cross sections and fittings are decided by acceptable ranges. The fitting is done by changing all real and imaginary parameters of depth, radii, and the diffuseness. Once we obtain the suitable parameters, depth and radii are kept fixed, and diffuseness parameter is changed in steps of 0.03 fm. All these fits are equally good to describe the angular distribution and represent families to optical potential parameters. Therefore we evaluate potential at sensitivity radii Rsr and Rsi [10], which is defined as the value at which different good fits possess the same value. The value of average real and imaginary radii was found to be 9.4 fm. The crossing radius for real and imaginary potentials are demonstrated in figure 3.4 corresponding to energies 14 MeV and 12 MeV.

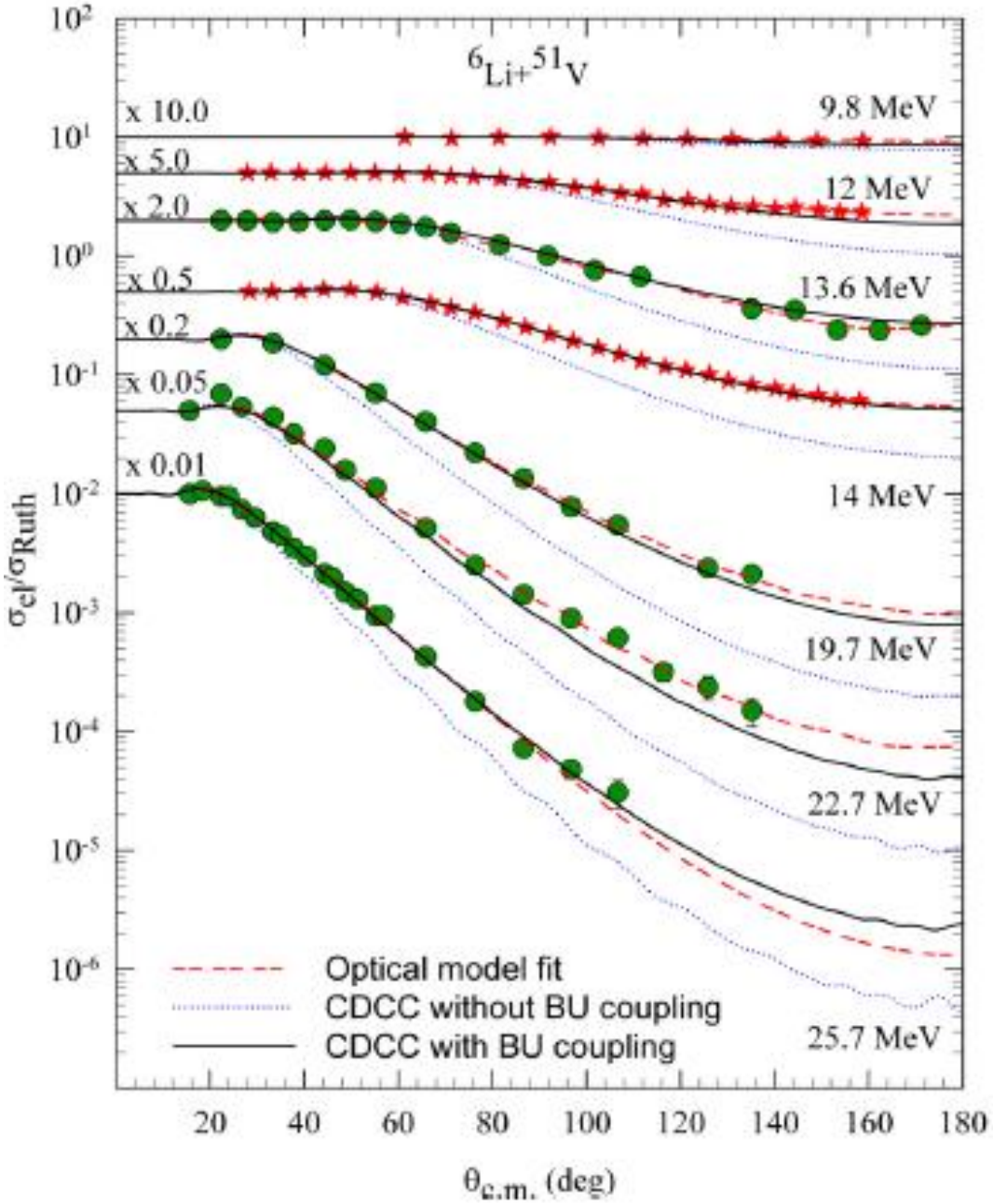

Figure 3.3: *Elastic scattering angular distribution data fitting through Woods –Saxon potential (WSP). Circles are deduced from present measurements and data stars are taken from reference [8]. The optical model fittings are shown in red dashed lines.*

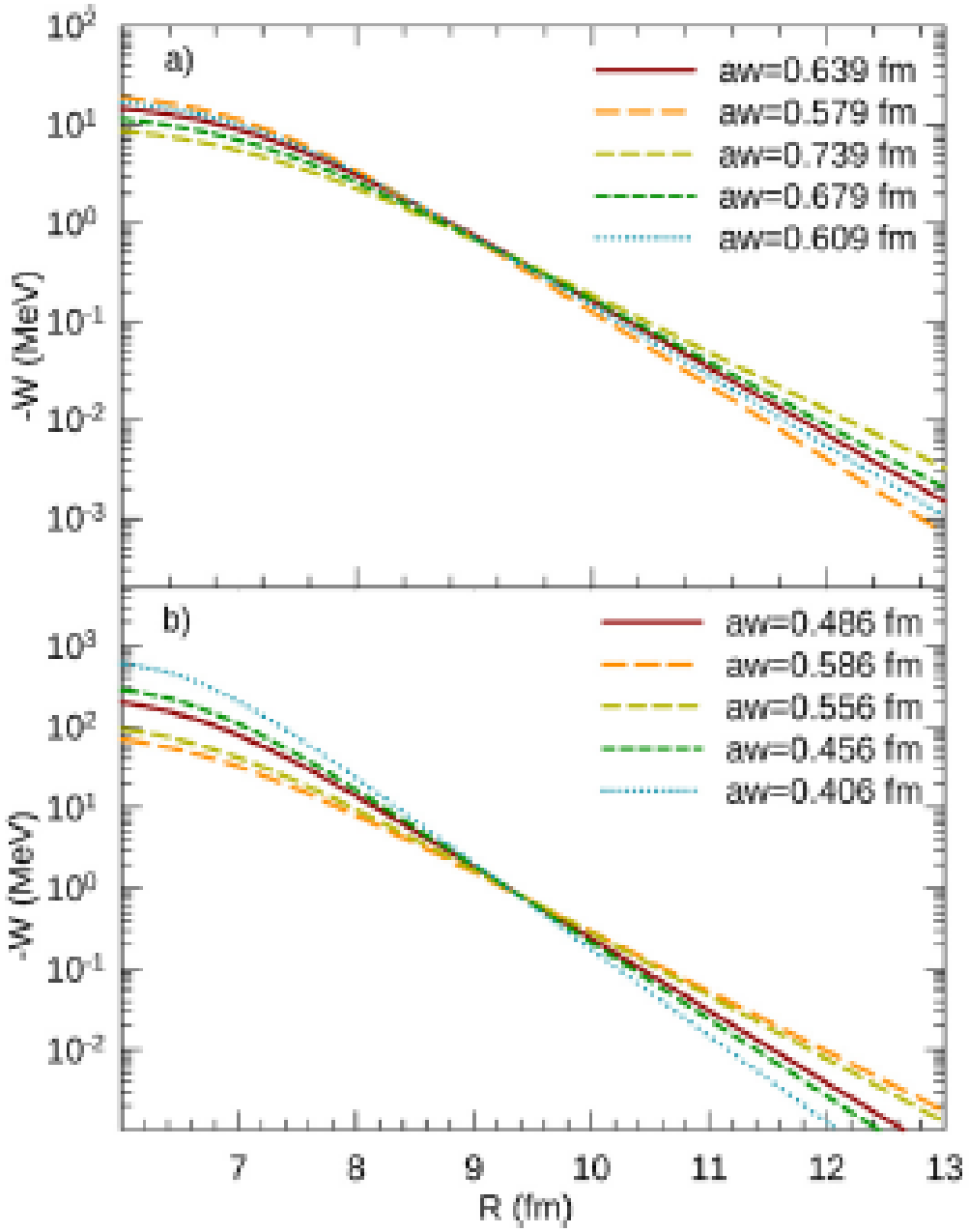

Figure 3.4: *The sensitivity radius deduced from optical model analysis for the imaginary part for the system $^{6}Li+^{51}V$ at energies a) 14 MeV b) 12 MeV.*

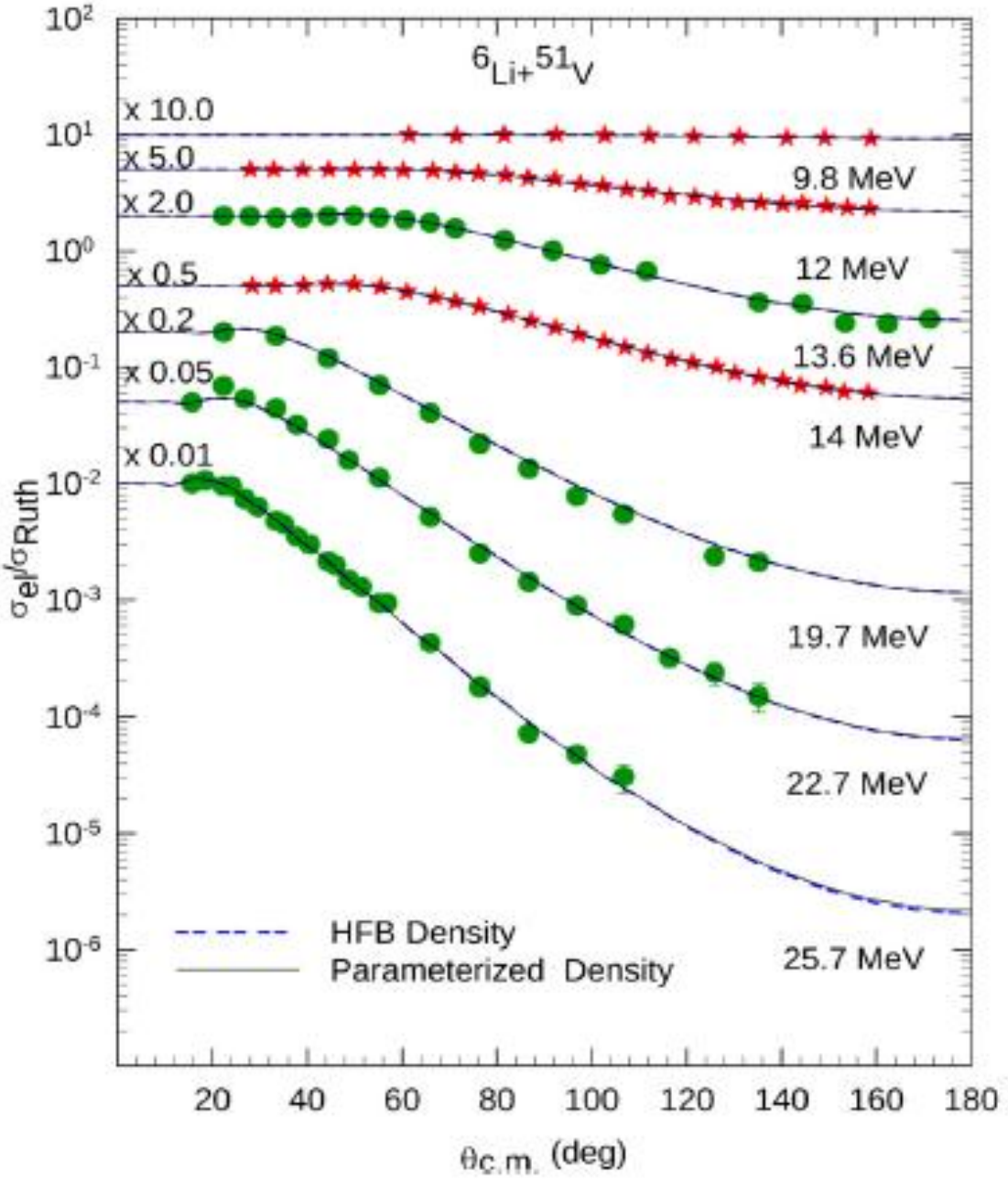

Figure 3.5: *Elastic scattering angular distribution data fitting through the microscopic double folding model. Circles are deduced from present measurements and data stars are taken from reference [8].*

3.3.2 Microscopic Double Folding Analysis

The double folding model integrates potential over nucleon density distribution using an effective M3Y nucleon-nucleon interaction potential as the detailed discussion is given in sec 2.4.2. For the present system, ^{6}Li nucleon density distribution was involved from reference [11] and that for ^{51}V is calculated using a static version of the Time Dependent Hartree Fock (TDHF) code Sky3D [12] as well as from two parameters Fermi distribution deduced from electron scattering data [13]. Further the matter distribution generation and conclusive calculation of folding potential from density distribution obtained from the utilization of HFB in DFPOT [14]. Thus with help of SFRESCO elastic scattering data are fitted to deduce real (N_R) and imaginary (N_I) normalization parameters using double folding potential from above method. The best fitted elastic scattering values are given in figure 3.5 and fitted N_R and N_I are given in Table 3.2.

3.3.3 Dispersion Calculation:

The discussion concerning dispersion relation calculation has been discussed in chapter 2 (section 2.4.2) in detail. The real (V(r, E)) and imaginary (W (r, E)) potentials are interrelated with a dispersion as follows,

$$\Delta V(r, E) = \frac{P}{\pi} \int_0^{\infty} \frac{W(r,E')}{E'-E}\, dE' \qquad (3.1)$$

And, $$V(r, E) = V_0(r, E) + \Delta V(r, E) \qquad (3.2)$$

ΔV (r, E) is obtained by W (r, E') which is made of considering imaginary potential divided into two or three liner segments. The imaginary part reflect an increase in potential before closing the reaction channel near the barrier region. A correlated dip in real portion is obtained from the dispersion calculation which is shown in figure 3.6. The shown errors are fitting errors.

3.3.4 CDCC Analysis

CDCC calculations play a significant role in investigating the breakup coupling effects of ^{6}Li by practicing the FRESCO code of version 3.1[9]. ^{6}Li (α+d) projectile, possess breakup threshold of 1.47 MeV. The continuum above that is discretized within momentum bins of width $\Delta k = 0.05$ fm^{-1}. In calculation, maximum limit for momentum was considered upto $k_{max}= 1.2$ fm^{-1} which corresponds to energy $E_{max}= 12.75$ MeV for $E_{lab}= 26$ MeV and $E_{max}= 5.65$ MeV for $E_{lab}= 9.8$ MeV. α+d cluster binding potential is extracted from reference [15], and potentials for d+^{6}Li and α+^{6}Li were taken from [16,17]. Real potential shape was considered in Woods-Saxon form. Imaginary potential was Woods –Saxon+ surface derivative potential. Imaginary surface potential strength was reduced by a factor of 0.5 for all energies and volume strength was further lessened by 0.5 times for 9.8 MeV energy to reproduce experimental results. A comparative study plot of experimental data with CDCC calculations is demonstrated in figure 3.3 with and without including breakup coupling effects to calculations. Solid lines depict the result of CDCC including breakup (BU) effects and dotted lines without BU effects. The impact of BU can be noticed at higher energies which gets a cautious reduction while energy approaches towards

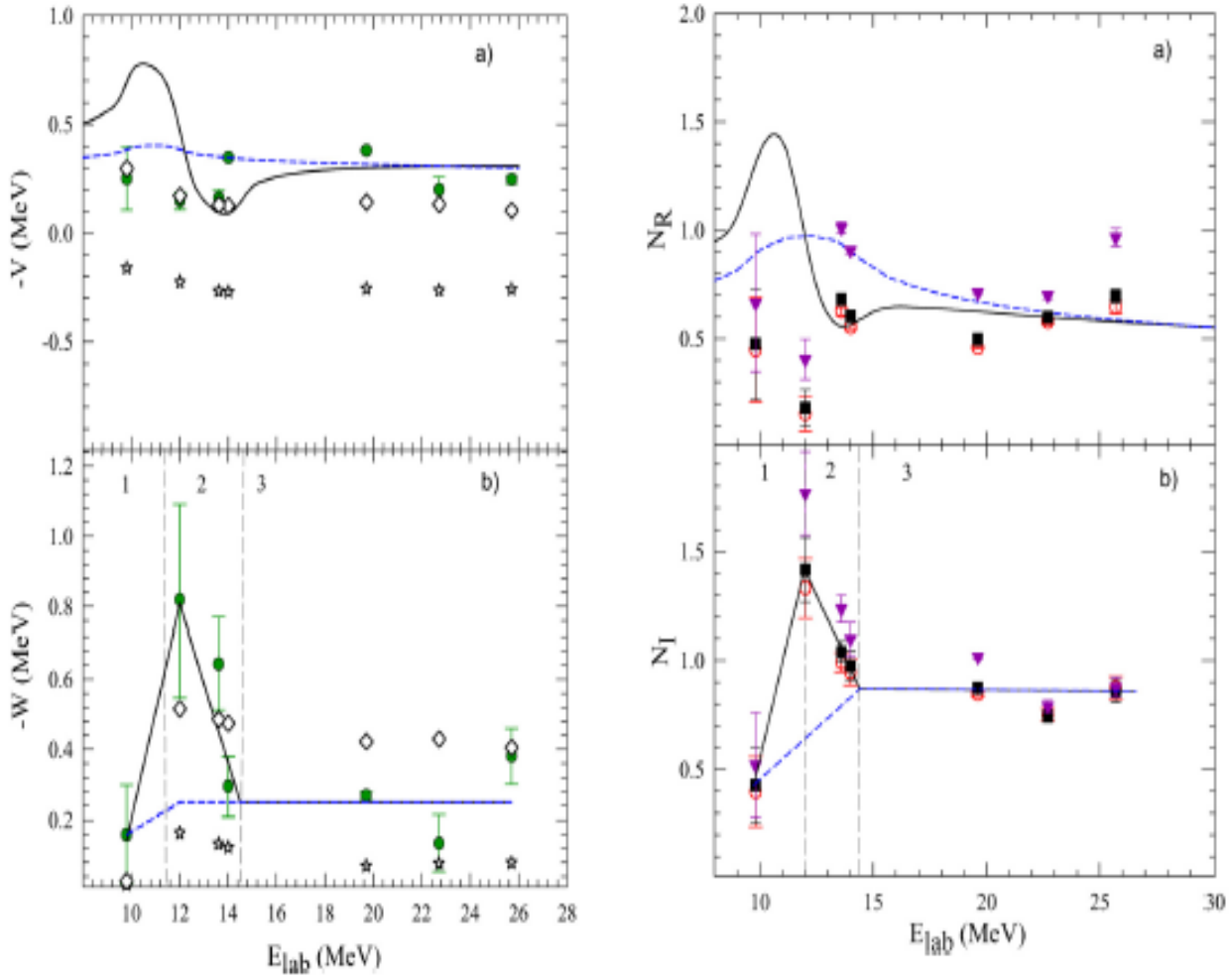

Figure 3.6: *Left panel: Real and imaginary potentials at sensitivity radius R=9.4 fm using optical model (solid circle). The dashed line represents two segment dispersion calculations and the solid line shows three segment dispersion calculations. Stars represent dynamic polarization potential (DPP) (ΔV, ΔW) and diamonds show bare + DPP, these calculations are obtained from CDCC calculations. Right Panel: Real (N_R) and imaginary (N_I) normalization factors from the microscopic double folding model. The lines represent dispersion calculations the same as in left panel.*

Table 3.1

Best fit optical potential parameters from elastic scattering data and N represents the number of data points.

E_{lab} (MeV)	V0 (MeV)	r_v (fm)	av (fm)	W_0 (MeV)	R_w (fm)	aw (fm)	σ_R (mb)	X^2/N
25.7	43.74	1.172	0.565	9.55	1.206	0.860	1486±51	1.07
22.7	35.76	1.188	0.537	38.44	0.985	0.689	1199±108	3.71
19.7	38.27	1.198	0.604	8.03	1.340	0.593	1057±39	1.04
14.0	55.57	1.258	0.480	48.61	0.930	0.830	574±27	0.23
13.6	40.67	1.277	0.419	1.43	1.672	0.637	553±19	0.83
12.0	11.82	1.279	0.522	26.34	1.266	0.692	273±26	0.58
9.8	18.92	1.286	0.532	3.95	1.253	0.780	19±8	0.63

Table 3.2

The normalization factors N_R and N_I for real and imaginary parts of the double folding potential, determined with SFRESCO.

E_{lab} (MeV)	N_R	N_I	X^2/N	σ_R^{DF}	σ_R^{CDCC}	σ_R^{BU}	σ_{NR}^{BU}	σ^{DF}total
25.7	0.70	0.87	2.6	1487±42	1448	70.8	15.2	86
22.7	0.60	0.80	8.15	1250±53	1315	69.1	14.9	84
19.7	0.50	0.88	0.81	1201±70	1142	106.5	16.5	123
14.0	0.61	0.99	0.26	586±32	56	138.2	4.8	143
13.6	0.69	1.05	1.03	547±23	509	81.6	3.4	85
12.0	0.18	1.42	0.58	295±24	275	22.2	1.8	24
9.8	0.48	0.43	0.64	19±7	17.5	1.81	0.21	2.02

barrier. Breakup effect is also shown in figure 3.7, the trend of polarization potential, which is inferred from breakup coupling, exhibits attractive behaviour for imaginary potential and repulsive behaviour for real potential.

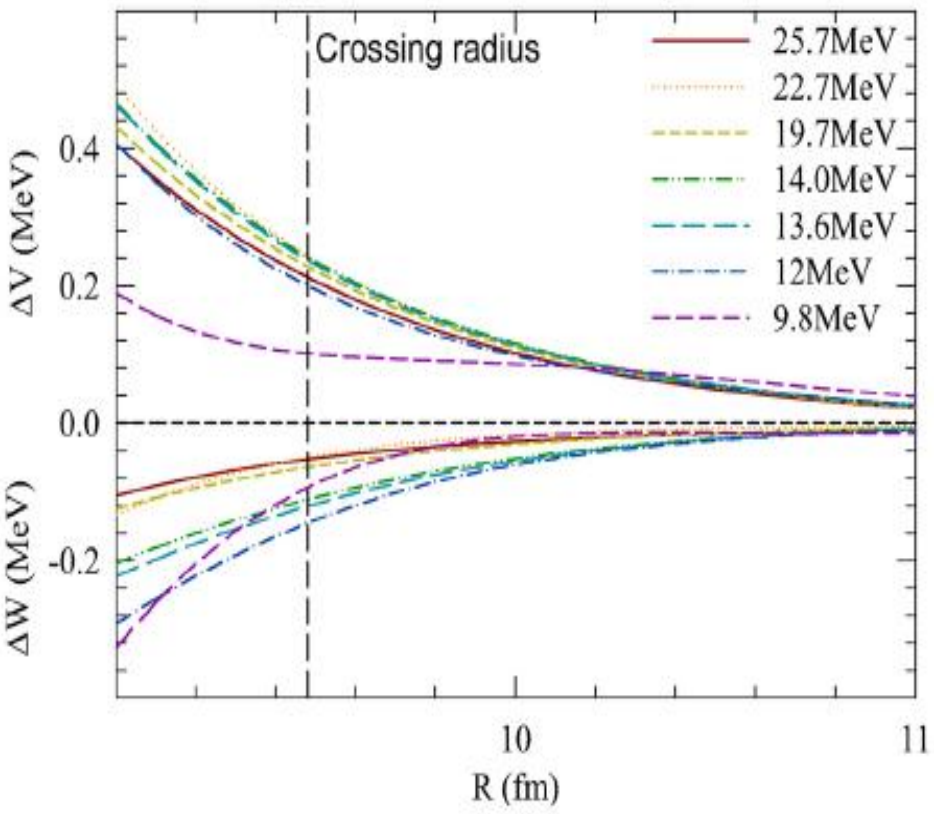

Figure 3.7: *Result of CDCC calculation for real (ΔV) and imaginary (ΔW) polarization potential around sensitivity radius (9.4 fm).*

3.4 Systematic studies

3.4.1 Systematics of Dispersion Calculation:

A systemized study of dispersion relation was investigated to explore the mass dependence of potential for varying mass range targets. The target density distribution was calculated from theoretical HFB densities using Time Dependent Hartree Fock (TDHF) code Sky3D [12] to make distribution parameter free and experimental parameterized electron scattering experiments [13] in double folding framework. ^{6}Li Projectile density was taken from Bray et al. [18]. Double folding model was used to calculate real potential and imaginary potential was kept same as that of real. This way deduced real (N_R) and imaginary (N_I) normalization factors are plotted for lighter to heavier mass range targets in figure 3.8. All the systems show an increase in N_I near their barrier region and thus replicate the signature of Break up Threshold Anomaly (BTA). The 2- segments for imaginary potential don't describe the data for real potential behavior.

3.4.2 Systematics of Reaction Cross- Section

The vanishing of geometrical effects of participating nuclei quantities such as cross section and energy are reduced and systemization of projectile and target is done in the scale and shown in figure 3.9. Adopting the reduction technique from reference [33], reduced cross section $\sigma/(A_P^{(1/3)} + A_T^{(1/3)})^2$ is plotted against reduced energy $E_c (A_P^{(1/3)} + A_T^{(1/3)}) / Z_P Z_T$ where σ is cross section, T, P denote target, projectile individually. The reduced experimental data yet reflect little spreading and thus to reduce its energy is reduced with the Coulomb barrier as $E_{c.m.}/ V_B$ which is shown in the lower panel and gives less spread of the cross section.

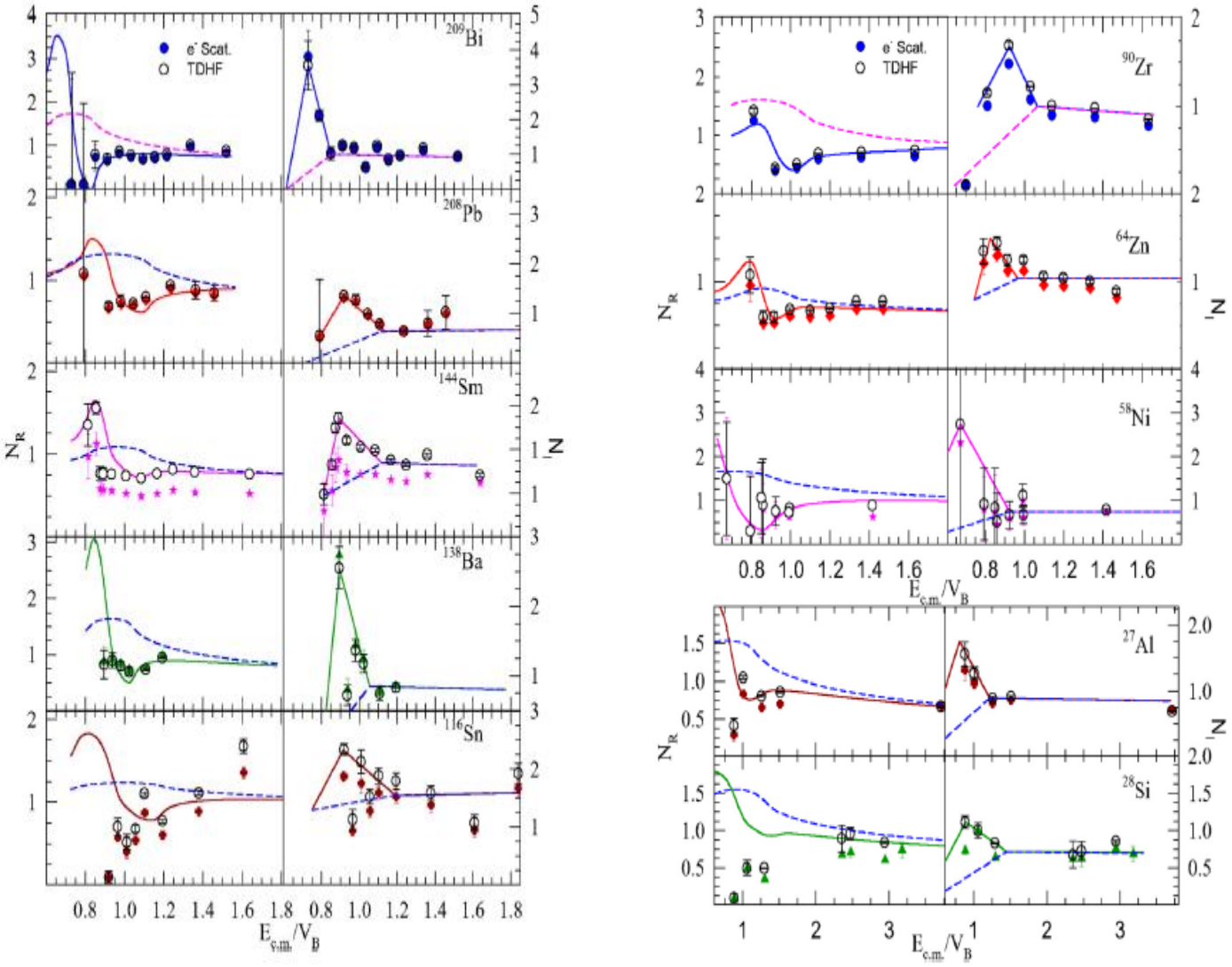

Figure 3.8: *Real and Imaginary normalization factors for systems $^{6}Li+^{27}Al$ [19, 20], ^{28}Si [21, 22, 23], ^{58}Ni [24, 25], ^{64}Zn [26], ^{90}Zr [3], ^{116}Sn [27], ^{138}Ba [28], ^{144}Sm [29], ^{208}Pb [30, 31], ^{209}Bi [32].*

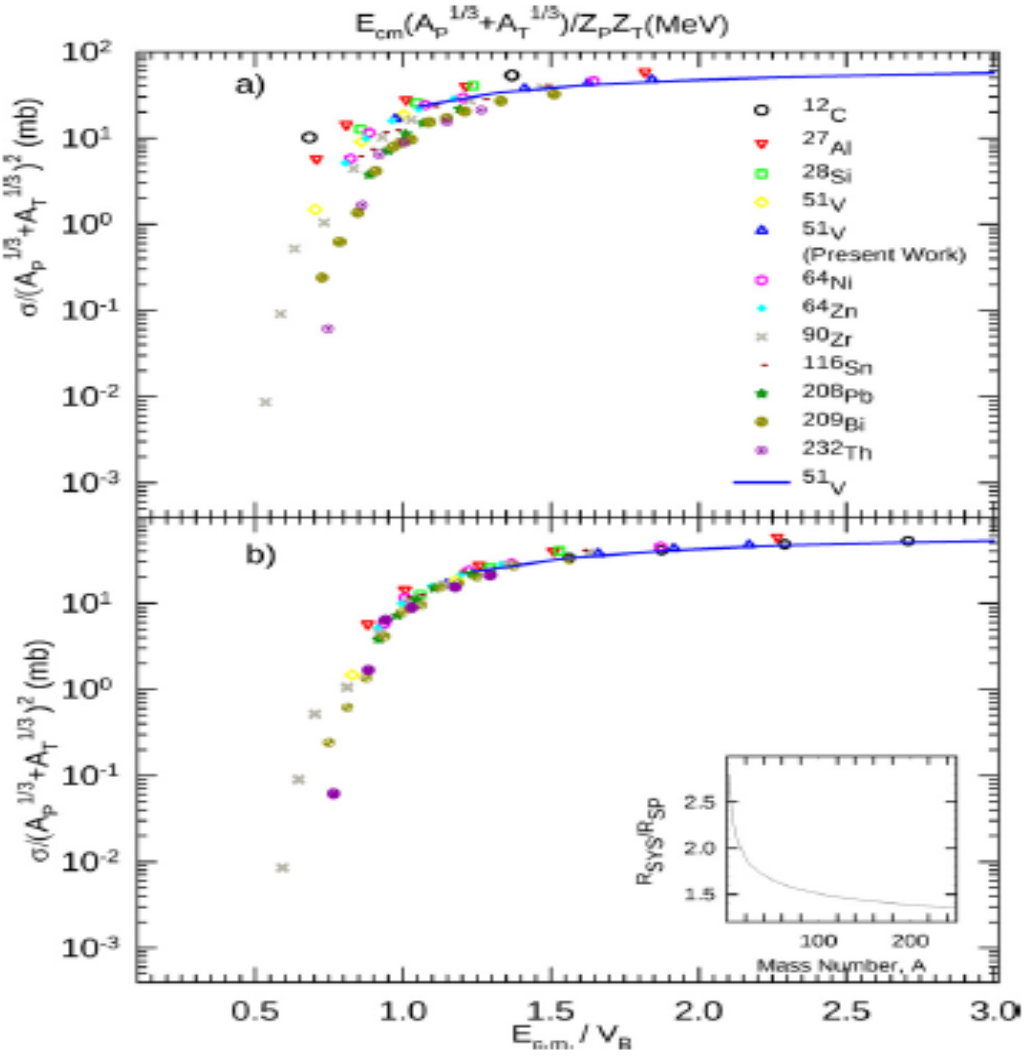

Figure 3.9: *(a) Reduced reaction cross section for targets from different mass regions with ^{6}Li. Reduction formulas for energy are mentioned on the axis. The Solid line is the systematic calculation from reference [34]. (b) Reduced reaction cross section with energy reduced as on formula at bottom scale. The cross section values were adopted from references [35, 19, 21, 8, 25, 26, 3, 27, 30, 32, 36]. The ratio of systematic radius $R^{i}_{sys}= 1.12A_i^{1/3} – 0.96\ A_i^{-1/3} + 3.75$ fm to spherical radius $R^{i}_{SP} = 1.3\ A_i^{1/3}$ fm is given in the inset.*

Along with that ratio of radius in Bass systematics to spherical radius is plotted against mass A number which demonstrates a significant drop in barrier height for lighter nuclei than for heavier nuclei. The total reaction cross section for the current system was theoretically calculated using the universal parameterization of total cross section. [34]. A systematic study of strongly bound projectiles (SBP), weakly bound projectiles (WBP), Radioactive Ion Beams (RIB) with ^{51}V was studied as demonstrated in figure 3.10. Low breakup threshold and WBP show higher cross sections, RIB/ exotic nuclei further possess higher cross sections due to their extended structures/ radius.

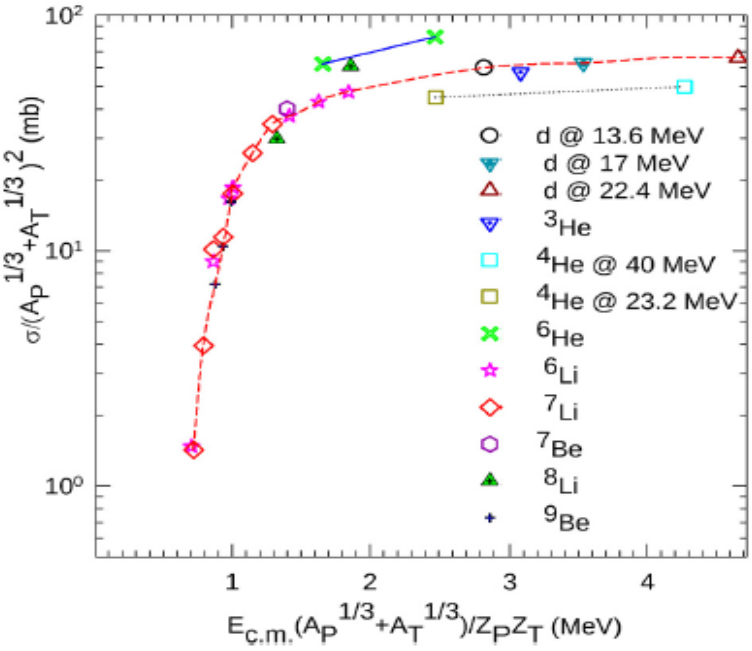

***Figure 3.10**: A systematic reaction cross section for a variety of projectile categories viz. strongly bound, Weakly bound, and rare ion beam with target ^{51}V. The cross sections are taken from reference [37-45, 8, 46, 47]*

3.5 Summary and conclusion

In present study, elastic scattering angular distribution of light mass system ^{6}Li+^{51}V nearby Coulomb barrier energies has been investigated. This measurement has been worked out in the phenomenological model, optical model, and CDCC calculation frameworks. The present system exhibits breakup threshold anomaly as a near barrier rise can be observed in imaginary part and a corresponding dip in real part. Elastic scattering measurements were properly produced by the breakup coupling effect in the three body CDCC model computation. Although, in comparison to Double Folding (DF) potential analysis, the polarization potential derived from these calculations differs somewhat. The possible reason may be the approximation method used in CDCC analysis. Dynamic polarization potential is repulsive for real part and attractive for imaginary part. Further, using HFB model densities and a DF potential framework, the mass dependence of BTA was investigated. and was resulting into the same conclusion. The same framework was used for mass ranging lighter to heavier. A systemization of reaction cross section for ^{6}Li was drawn to conclude a universal behavior. Reaction cross sections for SBP, WBP, and RIBs with 51V were systematically analyzed. With a growing trend, it shows the lowered reaction cross-sections from SBP to RIB, which are influenced by lower binding energy, cluster structure, and halo structure.

References

[1] J. Lei, A.M. Moro, Phys. Rev. C 95 (2017) 044605.

[2] K. Rusek, I. Martel, J. Gómez-Camacho, A.M. Moro, R. Raabe, Phys. Rev. C 72 (2005) 037603.

[3] A. Lemasson, A. Navin, M. Rejmund, N. Keeley, V. Zelevinsky, S. Bhattacharyya, A. Shrivastava, D. Bazin, D. Beaumel, et al., Phys. Lett. B 697 (2011) 454.

[4] J.P. Fernández-García, A. DiPietro, P. Figuera, J. Gómez-Camacho, M. Lattuada, J. Lei, A.M. Moro, M. Rodríguez-Gallardo, V. Scuderi, Phys. Rev. C 99 (2019) 054605.

[5] H. Kumawat, C. Joshi, V. V. Parkar, V. Jha, B. J. Roy, Y. S. Sawant, P. C. Rout, E. T. Mirgule, R. K. Singh, N. L. Singh *et al.*, Nucl. Phys. A **1002**, 121973 (2020).

[6] https://www.tifr.res.in/~pell/plf25_2013.pdf

[7] A. Chatterjee, LAMPS: Linux advanced multiparameter system, http://www.tifr.res .in /~pell

[8] K.H. Mobius, R. Bottger, P. Egelhof, Z. Moroz, E. Steffens, G. Tungate, Z. Phys. A 306 (1982) 335.

[9] I.J. Thompson, FRESCO, version FRES3.1, http://www.fresco .org .uk /source /fres -v31 .html, 2019.

[10] G.R. Satchler, Phys. Rep. **199**, 147 (1991).

[11] G.C. Li, I. Sick, R.R. Whitney, M.R. Yearian, Nucl. Phys. A 162 (1971) 583.

[12] J.A. Mahurn, P.G. Reinhard, P.D. Stevenson, A.S. Umar, Comput. Phys. Commun. 185 (2014) 2195.

[13] H.D. Vries, C.W. Dejager, C.D. Vries, At. Data Nucl. Data Tables 36 (1987) 495.

[14] J. Cook, Comput. Phys. Commun. 25 (1982) 125.

[15] K.I. Kubo, M. Hirata, Nucl. Phys. A 187 (1972) 186.

[16] H. An, C. Cai, Phys. Rev. C 73 (2006) 054605.

[17] V. Avrigeanu, M. Avrigeanu, EPJ Web Conf. 2 (2010) 02003.

[18] K.H. Bray, M. Jain, K.S. Jayaraman, G. Lobianco, G.A. Moss, W.T.H. Vanoers, D.O. Wells, Nucl. Phys. A 189 (1972) 35.

[19] J.M. Figueira, J.O. FernándezNiello, D. Abriola, A. Arazi, O.A. Capurro, E. deBarbará, G.V. Martí, D. MartínezHeimann, A.E. Negriet, et al., Phys. Rev. C 75 (2007) 017602.

[20] G. Ciangaru, R. McGrath, F. Cecil, Nucl. Phys. A 380 (1982) 147.

[21] A. Pakou, N. Alamanos, A. Lagoyannis, A. Gillibert, E. Pollacco, P. Assimakopoulos, G. Doukelis, K. Ioannides, D. Karadimos, et al., Phys. Lett. B 556 (2003) 21.

[22] M. Sinha, H. Majumdar, P. Basu, S. Roy, R. Bhattacharya, M. Biswas, M. Pradhan, R. Palit, I. Mazumdar, S. Kailas, Eur. Phys. J. A 17 (2011) 03004.

[23] M. Hugi, J. Lang, R. Muller, E. Ungricht, Nucl. Phys. A 368 (1981) 173.

[24] E.F. Aguilera, E. Martinez-Quiroz, D. Lizcano, A. Gómez-Camacho, J.J. Kolata, L.O. Lamm, V. Guimarães, R. Lichtenthäler, O. Camargo, F.D. Becchetti, H. Jiang, P.A. DeYoung, P.J. Mears, T.L. Belyaeva, Phys. Rev. C 79 (2009) 021601.

[25] M. Biswas, S. Roy, M. Sinha, M. Pradhan, A. Mukherjee, P. Basu, H. Majumdar, K. Ramachandran, A. Shrivastava, Nucl. Phys. A 802 (2008) 67.

[26] M. Zadro, P. Figuera, A. DiPietro, F. Amorini, M. Fisichella, O. Goryunov, M. Lattuada, C. Maiolino, A. Musumarra, Phys. Rev. C 80 (2009) 064610.

[27] N.N. Deshmukh, S. Mukherjee, D. Patel, N.L. Singh, P.K. Rath, B.K. Nayak, D.C. Biswas, S. Santra, E.T. Mirguleet, et al., Phys. Rev. C 83 (2011) 024607.

[28] A.M.M. Maciel, P.R.S. Gomes, J. Lubian, R.M. Anjos, R. Cabezas, G.M. Santos, C. Muri, S.B. Moraes, R. LiguoriNetoet, et al., Phys. Rev. C 59 (1999) 2103.

[29] J.M. Figueira, J.O. FernándezNiello, A. Arazi, O.A. Capurro, P. Carnelli, L. Fimiani, G.V. Martí, D. Mar-tinezHeimann, A.E. Negriet, et al., Phys. Rev. C 81 (2010) 024613.

[30] N. Keeley, S.J. Bennett, N.M. Clarke, B.R. Fulton, G. Tungate, P.V. Drumm, M.A. Nagarajan, J.S. Lilley, Nucl. Phys. A 571 (1994) 326.

[31] Z. Chun-Lei, Z. Huan-Qiao, L. Cheng-Jian, R. Ming, L. Zu-Hua, Y. Feng, W. Xiu-Kun, Z. Ping, A. Guang-Penget, et al., Chin. Phys. Lett. 23 (2006) 1146.

[32] S. Santra, S. Kailas, K. Ramachandran, V.V. Parkar, V. Jha, B.J. Roy, P. Shukla, Phys. Rev. C 83 (2011) 034616.

[33] P.R.S. Gomes, J. Lubian, I. Padron, R.M. Anjos, Phys. Rev. C 71 (2005) 017601.

[34] R. Tripathi, F.A. Cucinotta, J.W. Wilson, Nucl. Instrum. Methods Phys. Res., Sect. B 117(4) (1996) 347–349.

[35] J.E. Poling, E. Norbeck, R.R. Carlson, Phys. Rev. C 5 (1972) 6.

[36] S. Dubey, S. Mukherjee, D.C. Biswas, B.K. Nayak, D. Patel, G.K. Prajapati, Y.K. Gupta, B.N. Joshi, L.S. Danuet, et al., Phys. Rev. C 89 (2014) 014610.

[37] O.M.P. Bilaniuk, V.V. Tokarevskii, V.S. Bulkin, L.V. Dubar, O.F. Nemets, L.I. Slyusarenkoet, et al., Phys. G, Nucl. Phys. 7 (1981) 1699.

[38] J.D. Childs, W.W. Daehnick, M.J. Spisak, Phys. Rev. C 10 (1974) 217.

[39] B. Wilkins, G. Igo, Phys. Lett. 3 (1962) 48.

[40] S. Mayo, W. Schimmerling, M.J. Sametband, R.M. Eisberg, Nucl. Phys. 62 (1965) 393.

[41] J. Testoni, J. Rosenblatt, S. Mayo, Nucl. Phys. 74 (1965) 481.

[42] A. Korff, P. Haefner, C. Baumer, A.M. vandenBerg, N. Blasi, B. Davids, D. DeFrenne, R. deLeo, D. Frekerset, et al., Phys. Rev. C 70 (2004) 067601.

[43] G.W. Greenlees, J.S. Lilley, P.C. Rowe, P.E. Hodgson, Nucl. Phys. 24 (1961) 334.

[44] G. Igo, B.D. Wilkins, Phys. Rev. 131 (1963) 1251.

[45] S. Mukherjee, N.N. Deshmukh, V.G. aes, J. Lubian, P.R.S. Gomes, A. Barioni, S. Appannababu, C.C. Lopes, E.N. Cardozoet, et al., Eur. Phys. J. A 45 (2010) 23.

[46] R. Lichtenthäler, P.N. de Faria, A. Lépine-Szily, V. Guimarães, O. Camargo, R. Denke, E.A. Benjamim, A. Barioni, K.C.C. Pires, D.L. Mendes, M. Assunção, A. Arazi, I. Padron, P.R.S. Gomes, Eur. Phys. J. Spec. Top. 150 (2007) 27.

[47] J.C. Morales-Rivera, E. Martinez-Quiroz, T.L. Belyaeva, E.F. Aguilera, D. Lizcano, P. Amador-Valenzuela, EPJ Web Conf. 117 (2016) 07027.